



Investigation in The Close-Ground Characteristics of Torsional Damping Flap

Yuanzhi Qian^{1,2,*}, Tianjun Zhu¹, Zunling Du¹, Zhifeng Wu¹, Jianguo Liang¹

1 College of Mechanical and Automotive Engineering, Zhaoqing University, Zhaoqing, Guangdong, 526000, China; 2 Department of Mechanical Engineering, University of Bath, Bath, BA2 7AY, UK

*Corresponding to: Yuanzhi Qian

Abstract: Ground effects have a significant impact on road vehicles, particularly on blended wing body and lightweight designs. Racing vehicles participating in the World Solar Challenge fall into this category. A computational fluid dynamics (CFD) simulation was conducted for the NACA 0015 airfoil to investigate the effects of a torsional damping flap with ground effects. The analytical model demonstrated that an 1/4 chord-length torsional damping flap can reduce lift variation by 25%. However, the CFD results showed less efficacy because the analytical model was idealized using a thin plate model under no-slip conditions. In close-ground situations, the lift-alleviation performance of the flap is suppressed at low angles of attack but recovers at higher angles of attack, above 10 degrees. This behavior is attributed to the suppression of flow separation by the torsional damping flap.

Keywords: Torsional Damping Flap, Ground Effect, Blended-Wing Vehicle

1 INTRODUCTION

For vehicles operating close to the ground, such as aircraft during landing and take-off, significant lift and reduced induced drag can be generated due to ground effects. Additionally, ground effects can substantially enhance the lift-to-drag ratio, resulting in higher aerodynamic efficiency compared to normal flight at greater altitudes. The increased lift associated with ground effects can be attributed to the dynamic air cushion phenomenon, or impulse pressure, that occurs between the under-wing surface and the ground. Meanwhile, the reduction in induced drag is a result of decreased angle and strength of the downwash flow, as well as an increase in the equivalent spreading ratio influenced by ground effects [1]. Consequently, air vehicles that utilize ground effects can achieve greater flight range and lower fuel consumption, making them attractive for potential civil and military applications [2-3]. When an automobile is in motion, the aerodynamic effects between the vehicle's body and the ground can significantly influence its performance due to the vehicle's close proximity to the surface. Consequently, numerous studies have concentrated on the impact of ground effects on automobiles and trains [3-5]. Research conducted by Jinming et al. [3] revealed that the mechanisms behind ground effects on automobile lift are quite complex. They found that the relationship between ground

clearance and ground effect is not straightforward; thus, selecting the appropriate ground clearance based on the vehicle's operating conditions and the road surface can enhance vehicle stability. Additionally, Zhang et al. [4] explored the potential of utilizing ground effects to improve performance in racing cars. Their findings indicated that the aerodynamic design of Formula One cars intentionally leverages ground effects to enhance performance, resulting in lap time improvements of over 20% when these effects are effectively utilized.

One of the current trends in the automotive sector is energy efficiency and environmental protection, with electrification being a key revolution. Additionally, aerodynamic design has always significantly impacted vehicle performance. This is particularly true for commercial vehicles, but it is even more critical for racing cars. In the World Solar Challenge, an environmentally friendly automobile race, many cars have adopted various airfoil designs to accommodate solar panel installations and reduce aerodynamic drag. Although cars with airfoil cross-sections exhibit higher aerodynamic efficiency than conventional vehicle designs, they are also more vulnerable to wind gusts and ground effects [6-8]. Research on gust load reduction is quite extensive. Arredondo-Galeana et al. [9] proposed a passive flap that enables an airfoil to significantly mitigate load variations caused by gusts or airfoil oscillations. Qian et al. [10] and Bull et al. [11] explored the use of a spoiler to promote boundary layer separation, which effectively reduces

gust loads, achieving notable load reduction. The application of plasma jets [12] and air jets [13] to prevent boundary layer separation has also been investigated to mitigate gust-induced load changes. Additionally, various studies have focused on modifying the airfoil structure to reduce gust loads, including alterations to the overall design of the airfoil [14] and the incorporation of additional runners within the airfoil [15-16], both of which are viable methods.

Various gust load- alleviating devices have demonstrated their effectiveness in mitigating load variations across numerous studies. This indicates significant potential for applying such designs to ground vehicles, particularly solar cars equipped with various airfoil configurations. However, unlike airborne vehicles, ground vehicles are inherently influenced by ground effects, which means that the direct application of these load-alleviating devices does not guarantee their effectiveness. Among the different types of load-alleviating devices, movable trailing flaps have been selected due to their wide availability and proven performance in load alleviating. This study employs computational fluid dynamics to investigate the load-alleviating

capacity and mechanisms of a torsional damping flap under the influence of ground effects and gusty winds.

2 METHODOLOGIES

2.1 ANALYTICAL MODEL OF TORSIONAL DAMPING FLAP

The torsional damping flap is installed on a solar energy racing vehicle to alleviate the gust loads. The conceptual design of the racing vehicle is illustrated in Figure 1(a). The cross-section features a NACA 0015 airfoil with a chord length of 2000 mm. The designed body width is 1000 mm, with a minimum ground clearance of 300 mm, and fairings are present over the wheels and suspension system. The flap length is 500 mm, which is 1/4 of the chord length, and the rotation axle is located at 3/4 of the chord length of the airfoil (as shown in Figure 1(b)). Torsional springs are positioned between the main body of the airfoil and the flap, allowing the flap to adopt angles of attack that alleviate aerodynamic loads.

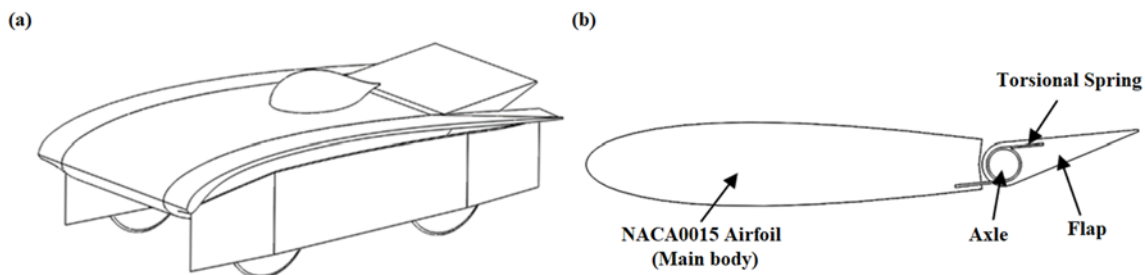


FIGURE 1: (A) CONCEPTUAL DESIGN OF THE SOLAR ENERGY VEHICLE, AND (B) CROSS-SECTION VIEW OF THE AIRFOIL VEHICLE BODY AND TORSIONAL DAMPING FLAP

For simplicity, we assume incompressible flow and no-slip conditions. Consequently, the wing can be represented as a thin plate. In this example, we will examine the variation of the angle of attack to assess the equivalent effects of gusts. First, we consider a rigid airfoil without flaps. As illustrated in Figure 2, the lift varies with different angles of attack. With an increase in the angle of attack, and under no-slip condition, there is no boundary layer separation, and the lift coefficient is proportional to 2π times the angle of attack. Therefore, the airfoil experiences an increase in lift ΔL .

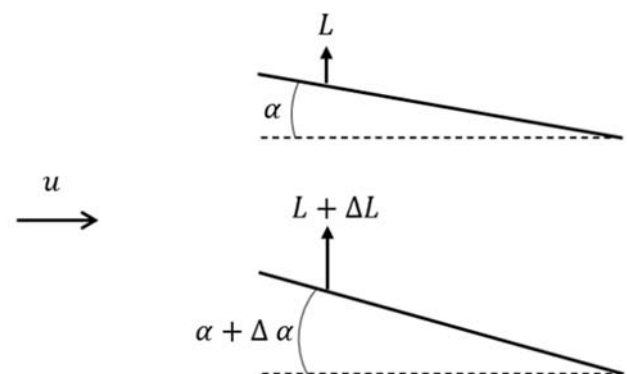


FIGURE 2: ANGLES OF ATTACK-LIFT VARIATION FOR A THIN PLATE

Now, we consider a quarter-chord length flap. At a given angle of attack, the flap will compress the torsional spring and remain level when it reaches torque balance. Figure 3 illustrates the

moment of force and how it changes with variations in the angle of attack.

At α degree angle of attack, the torsional spring is pre-tensioned to counterbalance the moment of lift from the flap M_p .

Thus,

$$M_p = M_s \tag{1}$$

and

$$L' = L * \frac{c - a}{c} \tag{2}$$

To note that we have

$$L_f = L * \frac{a}{c} \tag{3}$$

And

$$L' + L_f = L \tag{4}$$

Conditions remain consistent with those depicted in Figure 2 for a rigid airfoil without flaps.

With an increased angle of attack, the flap will rotate to a certain angle until balance is achieved:

$$M_s + \Delta M_s = M_p + \Delta M_p \tag{5}$$

At this point, the sectional lift of the leading part is

$$L' + \Delta L' \tag{6}$$

It is important to note that the total lift must include the contribution from the trailing part, the flap.

Here, we assume that to allow for the freedom of flap movement, the spring rate should be minimized. Additionally, to ensure that the flap is level with the main body of the airfoil at a specific angle of attack, the pre-tension angle must be significantly high to generate sufficient torque. Therefore, compared to $\Delta\theta$ when the flap rotates, the pre-tension angle θ is far higher. And we can assume

$$\theta + \Delta\theta \approx \theta \tag{7}$$

And

$$\Delta M_s = \Delta M_p \approx 0 \tag{8}$$

Based on that, we draw a conclusion

$$\Delta\alpha \approx \Delta\theta \tag{9}$$

from the force analysis in Figure 3. In this situation, L_f remains the same, while the total lift reduces to

$$(L + \Delta L) * \frac{c-a}{c} + L * \frac{a}{c} \tag{10}$$

(where a is flap chord length and c is the total chord length) with flap compared to

$$L + \Delta L \tag{11}$$

without the flap. The lift increment is also reduced from ΔL to

$$\Delta L * \frac{a}{c} \tag{12}$$

and we noticed that the lift alleviation is proportional to the length of the flap.

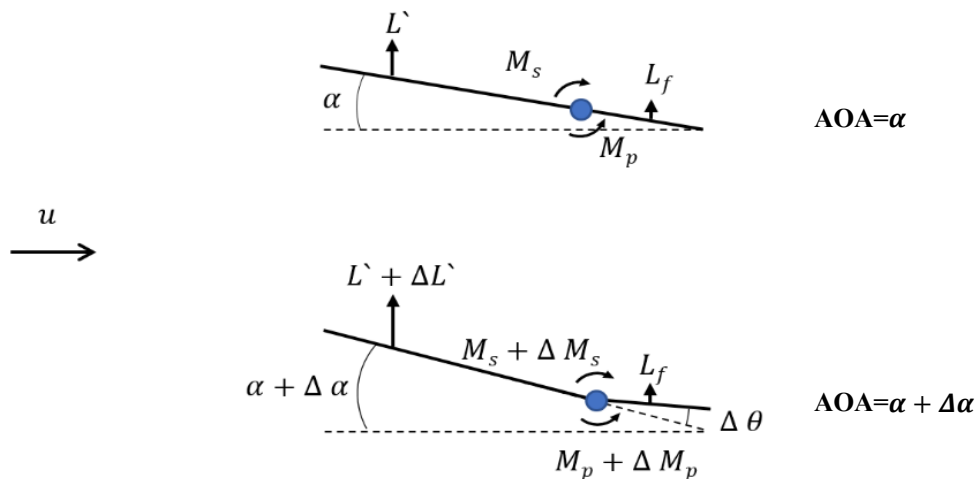


FIGURE 3: ANGLES OF ATTACK-LIFT VARIATION FOR A THIN PLATE WITH FLAP

Abbreviation in Figures 2&3:

α : Angle of attack

Δ : Increment

L : Lift force

L' : Sectional lift force of the airfoil main body

L_f : Sectional lift force of the flap

M_s : Moment of spring pre-tension force

M_p : Moment of lift force from flap section

θ : Spring pre-tension angle

u : Freestream speed

2.2 COMPUTATIONAL FLUID DYNAMICS MODEL

The computational fluid dynamics section is conducted using Fluent and employs the Shear Stress Transport (SST) k-omega model, a two-equation vortex-viscous model that combines Wilcox's k-omega model with the k-epsilon model. The k-omega model is particularly effective for simulating flow within a viscous layer, making it suitable for calculations in the boundary layer. In contrast, the k-epsilon model excels at predicting flow behavior in regions away from the wall. The selection of the appropriate model is governed by a mixing function, which enhances computational accuracy [17]. The governing equations of the SST k-omega model encompass the turbulent kinetic energy equations and the specific dissipation rate equations. The improved SST k-omega model proposed by Menter et al. [18] is utilized, ensuring that the equations and model parameters are consistent with this enhancement.

The blended-wing body and movable flap will be mounted on the solar race car, as illustrated in Fig. 1(a). Despite the small wingspan, the presence of wheel fairings on both sides, which block downwash airflow, allows for the use of a 2D model in the calculations. The grid utilized for the calculations is depicted in Fig. 4. A dynamic mesh is employed for the movable tail section, with the rotor axis positioned at 3/4 of the chord length (c).

The torsion spring constant was set to $k = 0$ N/m, and the moment of inertia, based on previous assumptions and the design materials, yielded $I_z = 0.02$ kg·m². A wall was positioned below the wing to simulate the ground surface, corresponding to the front edge of the wing, and extending all the way to the far field at the rear. The test simulates a vertical gust of wind generated by a solar race vehicle traveling at a constant cruising speed of $u = 15$ m/s, which is close to the average cruising speed of race vehicles in the World Solar Challenge. The Reynolds number based on the chord length is $Rec = 2 \times 10^6$.

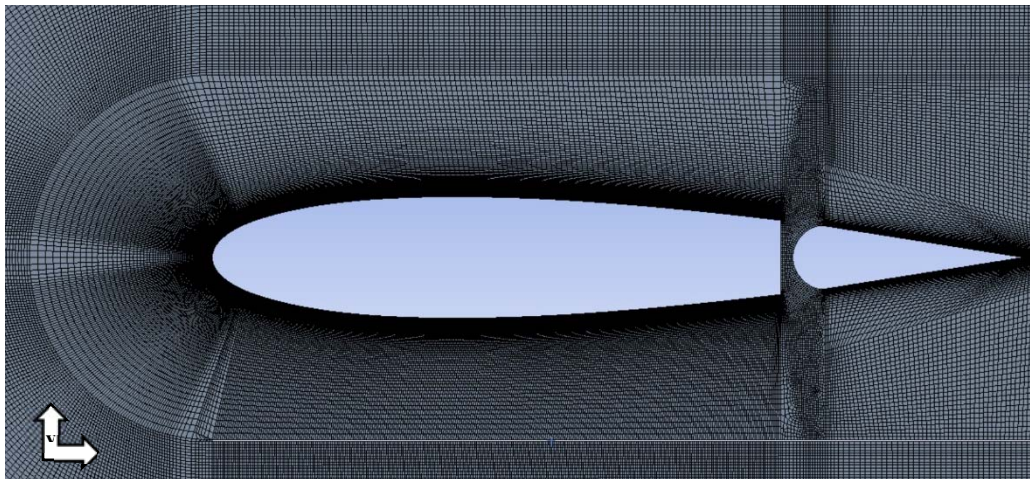


FIGURE 4: MESH FOR CFD

3 RESULTS AND DISCUSSION

Figure 5 compares the coefficient of lift (CL) for various configurations of NACA0015 airfoils at steady state across different angles of attack. The results from Zanon [19] indicate a critical Reynolds number (Rec) of 1.5×10^6 , while the other configurations exhibit a Rec of 2×10^6 . In the figure, the blue dotted line represents the NACA0015 airfoils modeled without a separated flap structure, meaning there is no joint between the main body and the flap. In contrast, all other models, except for Zanon's results represented by the dotted line, include a flap. The key difference lies in whether the flap is permitted to rotate in CFD. It is evident that the experimental model depicted by the blue dotted line closely aligns with the results of other studies that have similar Reynolds numbers, suggesting that this model is viable for practical applications. In the case of the fixed flap in freestream, seam between the flap and the main airfoil body results in a reduced lift coefficient compared to the seamless configuration, particularly at higher angles of attack. This

reduction occurs because the seam facilitates the transfer of high pressure from the lower surface to the upper surface, diminishing the pressure difference between the upper and lower airfoils. This effect becomes more pronounced as the angle of attack increases, which aligns with theoretical expectations. Reason: Improved clarity, vocabulary, and technical accuracy while maintaining the original meaning.

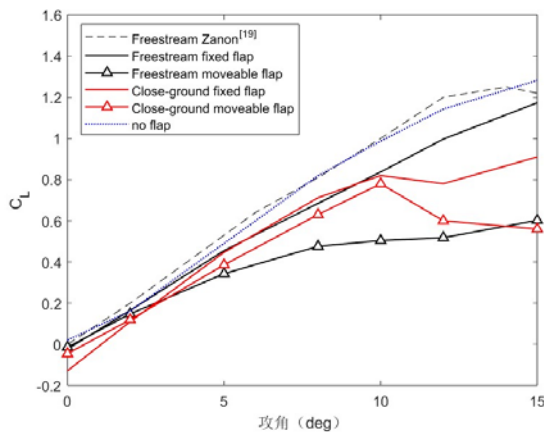


FIGURE 5: LIFT COEFFICIENT AGAINST ANGLE OF ATTACK

Figure 6 compares the velocity magnitude flow field plots of the airfoil for various steady-state cases with different angles of attack, with or without tail movable, and with or without near-wall surface. In the free-flow case away from the wall (left column of Fig. 6), at an angle of attack of 0° , whether the tail is movable or not did affect the flow field and tail oscillations, and no significant difference was found when combined with the lift coefficients in Fig. 5. At an angle of attack of 10° , with the tail immovable, the boundary layer starts to show boundary layer separation near the tail, and the basic flow is as expected. Whereas at this angle of attack, the tail is allowed to move and reaches steady state with a tail rotation of about -3.5° (using clockwise rotation as a positive angle and counterclockwise rotation as a negative angle), whereas the boundary layer separation observed in the immovable tail is insignificant at this point, while there is a significant decrease in lift, which is more pronounced in this study compared to the theoretical model of Arredondo-Galeana et al [9], with a simultaneous the tail rotation angle is smaller. This is because their model is based on the thin-wing theory, and in the case shown in Fig. 5, a greater lift reduction can be achieved with a smaller rotation angle because the rotation of the trailing edge affects the separation of the boundary layer, and at the same time changes the trailing edge curvature resulting in a reduction of the downwash flow. Whereas close to the wall, even at an angle of attack of 0° , due

to the ground effect between the airfoil and the wall, which generates higher flow field velocities between them and results in negative lift, the movable tail will rotate by about 2° at this point to mitigate the effects of the airfoil due to its proximity to the wall. At high angles of attack, i.e., 10° , the fixed-tailed airfoil has a more pronounced boundary layer separation near the wall, as well as a pronounced low-speed region on the lower side of the airfoil's front, and such a near-ground effect ultimately results in stronger lift. Whereas, when the movable tail is used, the tail rotates about -5° , which is a larger rotation angle compared to the same angle of attack but non-near-wall case, which is also due to the presence of the wall resulting in a stronger lift of the airfoil.

4 CONCLUSIONS

The study investigates the impact of ground effects on the performance of a torsional damping flap in the context of solar racing vehicles. The conclusions drawn from the research indicate that while the analytical model suggested a 25% reduction in lift variation, the computational fluid dynamics (CFD) results showed less efficacy due to the differences between the idealized thin plate models and real-world conditions.

The ground effect significantly alters the behaviour of the flap, suppressing lift alleviation at low angles of attack but showing improvement at higher angles, particularly above 10 degrees. This behaviour arises from the flap's ability to influence flow separation, thereby altering the aerodynamic profile of the vehicle. When close to the ground, the effects become more pronounced, necessitating a larger rotation angle for the flap to maintain aerodynamic stability.

The study underscores the complexity of ground effect interactions and highlights the importance of using CFD for realistic modelling. The insights into how ground effects influence airfoil performance can aid in optimizing the design of solar racing vehicles, potentially leading to enhanced performance in terms of stability and efficiency. The findings are applicable not only to racing contexts but also hold potential for broader applications in vehicles operating near ground surfaces.

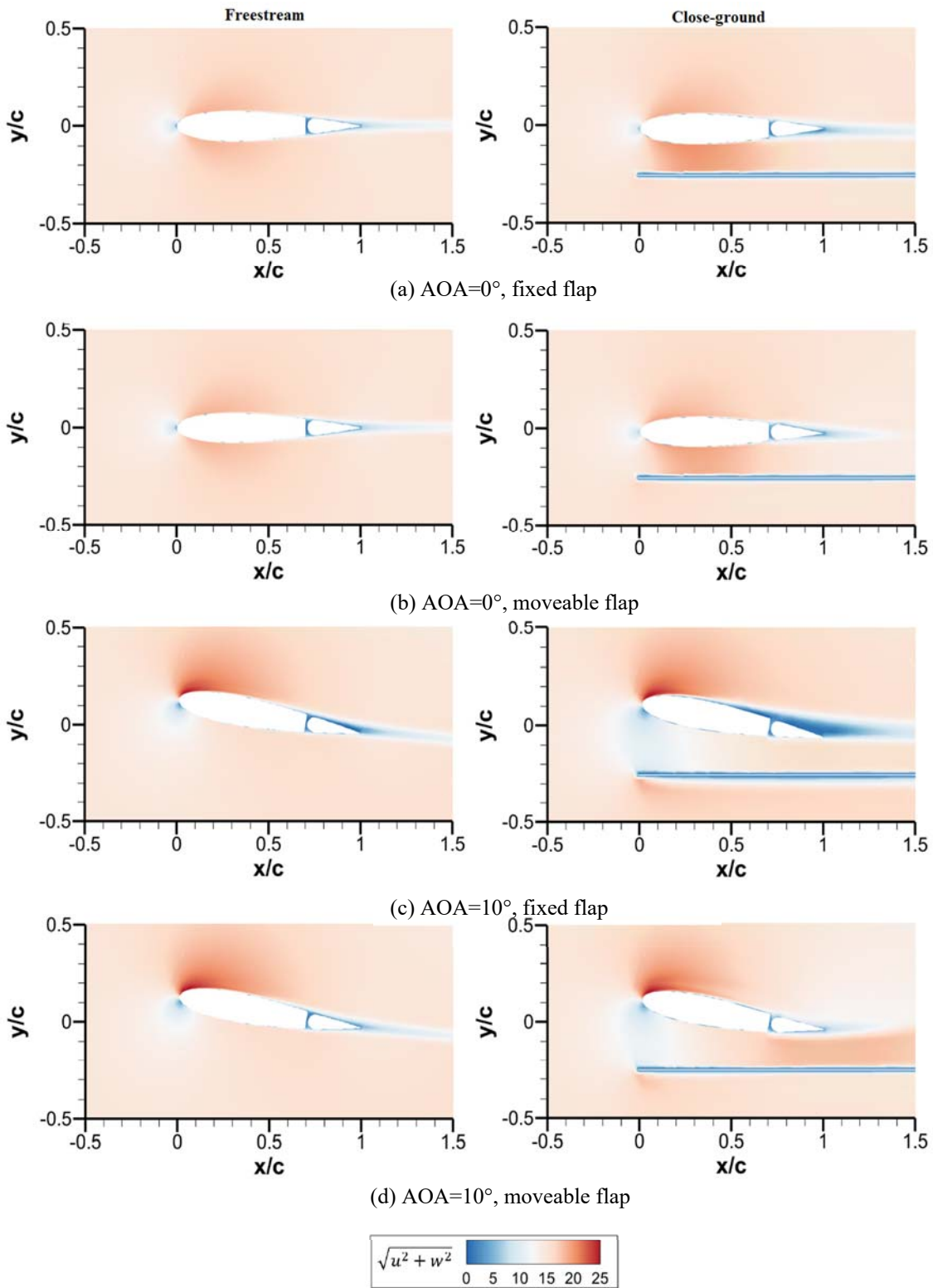


FIGURE 6: FLOW FIELD COMPARISONS

FUNDING

This research is funded by Zhaoqing University research fund (QN202342), NSFC research project (52372365) and Education



Department of Guangdong Province research project (2023ZDZX1032).

REFERENCES

- [1]Rozhdestvensky K V. Wing-in-ground effect vehicles[J]. Progress in aerospace sciences, 2006, 42(3): 211-283.
- [2]Birrell S A, Hooper R H, Haslam R A. The effect of military load carriage on ground reaction forces[J]. Gait & posture, 2007, 26(4): 611-614.
- [3]Jinming X, Yangjun Z, Shangrong T. Numerical simulation study of ground effects on flow field around vehicle bodies[J]. Chinese Journal of Mechanical Engineering, 2003, 39(3): 58-61.
- [4]Zhang X, Toet W, Zerihan J. Ground effect aerodynamics of race cars[J]. 2006.
- [5]Xia C, Shan X Z, Yang Z G, et al. Influence of ground effect in wind tunnel on aerodynamics of high speed train[J]. 2015.
- [6]Mangu R, Prayaga K, Nadimpally B, et al. Design, development and optimization of highly efficient solar cars: Gato del Sol I-IV[C]//2010 IEEE Green Technologies Conference. IEEE, 2010: 1-6.
- [7]Babalola P O, Atiba O E. Solar powered cars-a review[C]//IOP Conference Series: Materials Science and Engineering. IOP Publishing, 2021, 1107(1): 012058.
- [8]Tremblay-Dionne V, Lee T. Ground effect on the aerodynamics of a NACA 0015 airfoil with a plain trailing-edge flap[J]. Fluid. Mech. Res. Int. J., 2018, 2(1): 6-12.
- [9]Arredondo-Galeana A, Young A M, Smyth A S M, et al. Unsteady load mitigation through a passive trailing-edge flap[J]. Journal of fluids and structures, 2021, 106: 103352.
- [10]Qian Y, Wang Z, Gursul I. Lift alleviation in travelling vortical gusts[J]. The Aeronautical Journal, 2023, 127(1316): 1676-1697.
- [11]Bull S, Chiereghin N, Cleaver D J, et al. Novel approach to leading-edge vortex suppression[J]. AIAA Journal, 2020, 58(10): 4212-4227.
- [12]Post M L, Corke T C. Separation control using plasma actuators: dynamic stall vortex control on oscillating airfoil[J]. AIAA journal, 2006, 44(12): 3125-3135.
- [13]Greenblatt D, Wygnanski I. Dynamic stall control by periodic excitation, Part 1: NACA 0015 parametric study[J]. Journal of Aircraft, 2001, 38(3): 430-438.
- [14]Chandrasekhara M S, Wilder M C, Carr L W. Unsteady stall control using dynamically deforming airfoils[J]. AIAA journal, 1998, 36(10): 1792-1800.
- [15]Khodadoust A, Washburn A. Active control of flow separation on a high-lift system with slotted flap at high Reynolds number[C]//25th AIAA Applied Aerodynamics Conference. 2007: 4424.
- [16]Belamadi R, Djemili A, Ilinca A, et al. Aerodynamic performance analysis of slotted airfoils for application to wind turbine blades[J]. Journal of wind engineering and industrial aerodynamics, 2016, 151: 79-99.
- [17]Hellsten A. Some improvements in Menter's k-omega SST turbulence model[C]//29th AIAA, Fluid Dynamics Conference. 1998: 2554.
- [18]Menter F R, Kuntz M, Langtry R. Ten years of industrial experience with the SST turbulence model[J]. Turbulence, heat and mass transfer, 2003, 4(1): 625-632.
- [19]Zanon A. A vortex panel method for VAWT in dynamics stall[J]. 2011.